Eur. J. Mech. B/Fluids 18 (1999) 1027–1047

On pre-dissipative 'bumps' and a Reynolds-number-dependent spectral parameterization of turbulence

M. Coantic *, J.-J. Lasserre

I.R.P.H.E., U.M.R. 6594 C.N.R.S./Universités d'Aix-Marseille I & II, 12 Avenue Général Leclerc, 13003 Marseille, France

(Received 14 December 1998; revised 4 June 1999; accepted 11 June 1999)

Abstract – Considerable experimental, numerical and theoretical evidence has accumulated during the last two decades for the presence of a maximum above the right end of the inertial plateau in compensated high-Reynolds-number turbulence spectra $k^{+5/3}E(k)$. This energy pileup, due to the reduced nonlocal triadic interactions near the viscous cut-off, complies with Kolmogorov's 1941 theory but hampers experimental interpretation about its intermittency corrections. It has been included in a semi-empirical Reynolds-number-dependent complete (i.e. from the largest to the smallest scales) spectral model of isotropic turbulence. This simple parameterization is shown to represent satisfactorily well experimental data over a large variety of situations. © 1999 Éditions scientifiques et médicales Elsevier SAS

high Reynolds number turbulence / turbulence spectra / inertial subrange / Kolmogorov theory

1. Introduction

A.N. Kolmogorov's ideas have deeply influenced several generations of turbulence researchers (see Frisch [1] for a recent survey of Kolmogorov's 1941 (K 41) and 1962 (K 62) theories and their consequences). Any modern fluid dynamics textbook indicates that, after K 41, the intermediate and small scales of a turbulent flow with a sufficiently large Reynolds number display a universal locally isotropic behaviour entirely governed by the rate of viscous dissipation into heat of the kinetic energy of turbulence, ε, and by the fluid kinematic viscosity, ν. Furthermore, if the Reynolds number is very large, an 'inertial subrange' unaffected by viscosity has to be observed.

However, the basic theory provided neither figures as to the requested Reynolds numbers, nor numerical values for the spectral level and limits of the inertial subrange, nor expressions for the spectral behaviour of turbulence outside this subrange. These defects have since been the subject of a considerable amount of theoretical, experimental, and, more recently, numerical research (see Lesieur [2] for a review). The resulting classical spectral model, particularly well described in Tennekes and Lumley [3], presents power-law dependences less steep than $-5/3$ for wave numbers below the inertial subrange, equal to $-5/3$ in this subrange, and steeper than $-5/3$ above it. Consequently, plots of the 'compensated' turbulence spectra, of the form $k^{+5/3}E(k)$, as functions of the wave number k should display a more or less extended flat maximum, or plateau, in the inertial subrange and decrease on both sides of it.

In this paper, we will first review and discuss different data and arguments showing that the above picture is inexact. As we shall see, compensated turbulence spectra exhibit at the high wave number end of their inertial plateau, but at scales still not directly affected by viscous dissipation, a small but significant maximum. The

* Correspondence and reprints; coantic@marius.univ-mrs.fr

existence of this 'spectral bump' induces notable consequences, both fundamental and practical experimental ones.

In the range of Reynolds numbers most frequently encountered in experiments, this bump is in general mixed and confused with the low wave number spectral decrease resulting from the limitation in the size of the structures present in the flow. To overcome this difficulty, we will develop in the second part of the paper a new semi-empirical spectral representation covering the largest energy-containing to the smallest dissipative scale range. This representation is of course Reynolds number dependent and it is found to represent satisfactorily several features of the experimental data collected in a large variety of situations.

2. The classical model

We first need to review now for later use some well known data and derivations. As an immediate consequence of K 41, the scalar spectral function $E(k)$ displays a universal behaviour when rendered non-dimensional with the Kolmogorov length, $\eta = (\nu^3/\varepsilon)^{1/4}$, and velocity, $\upsilon = (\nu\varepsilon)^{1/4}$, scales, so that:

$$\widetilde{E}(\tilde{k}) = E(k)/(\upsilon^2\eta) = E(k)/(\varepsilon\nu^5)^{1/4} = f(\tilde{k} = k\eta) \tag{1}$$

is a universal non-dimensional function of the non-dimensional variable $\tilde{k}$. In the inertial subrange, ν has to disappear which produces as a consequence the celebrated minus five thirds law:

$$E(k) = \alpha\varepsilon^{2/3}k^{-5/3}, \quad \text{or} \quad \widetilde{E}(\tilde{k}) = \alpha\tilde{k}^{-5/3}, \tag{2}$$

where α is a universal constant, close to 1.6 after Sreenivasan's [4] recent compilation.

The shape of $E(k)$ is in fact governed by the dynamical spectral equation which, for a steady-state, isotropic (and therefore homogeneous) situation, is given by:

$$\frac{\partial}{\partial t}(E(k)) = 0 = T(k) - 2\nu k^2 E(k), \tag{3}$$

where $T(k) = 2\pi k^2 \iiint_{\mathbf{R}^3,\, \mathbf{k}+\mathbf{p}+\mathbf{q}=\mathbf{0},\, \|\mathbf{k}\|=k} T(\mathbf{k},\mathbf{p},\mathbf{q})\, d\mathbf{p}$ represents the integrated effect at wave number k of energy-conserving nonlinear inertial triad interactions, while the second term corresponds to the dissipative effect of viscosity. Usually, one represents $T(k)$ as minus the derivative of an energy-flux function $S(k)$ corresponding to the total inertial flux of energy from wave vectors with $\|\mathbf{k}\| < k$ to wave vectors with $\|\mathbf{k}\| > k$. From dimensional considerations, $S(k)$ can be written as: $S(k) = kE(k)/\alpha\tau(k)$, where $\tau(k)$ is an Onsager time scale (see, e.g., Lin [5]). The spectral equation then reads:

$$\frac{d}{dk}(S(k)) = \frac{d}{dk}\{kE(k)/(\alpha\tau(k))\} = -2\nu k^2 E(k), \tag{4}$$

which can be formally integrated as:

$$E(k) = \beta\alpha\varepsilon\frac{\tau(k)}{k}\exp\left(-2\nu\alpha\int_0^k k\tau(k)\,dk\right). \tag{5}$$

These results have to be compatible with the predictions of K 41, in particular in the inertial subrange where the direct effect of viscosity is negligible, so that (4) immediately leads to the conclusion that the inertial energy

flux stays practically equal to the rate of dissipation of energy:

$$S(k) \approx Cte = 2\nu \int_0^\infty k^2 E(k)\, dk = \varepsilon. \tag{6}$$

To obtain the inertial-range spectral law (2), it is therefore necessary for any closure of the dynamical equation (4) to predict a time scale $\tau(k)$ approaching the Corrsin–Pao expression: $\tau(k) = \varepsilon^{-1/3}k^{-2/3}$. If the latter is accepted in both the inertial and dissipation ranges, one thus gets the widely used Pao [6] spectrum, with the constant β equal to unity at large Reynolds numbers:

$$E(k) = \alpha\varepsilon^{2/3}k^{-5/3}\exp\left(-\frac{3}{2}\alpha\nu\varepsilon^{-1/3}k^{4/3}\right). \tag{7}$$

This result is typical of the semi-empirical closures which have been proposed before, say, 1970 (see, e.g., Hinze [7] for a review). The spectrum decreases as $k^{-5/3}$ in agreement with K 41 in the inertial range, then at a faster rate in the dissipation range due to the negative viscous destruction term in (4). The consideration of intermittency effects in K 62 and subsequent theories did not change much the admitted view that spectra decrease according to a power law with a constant negative exponent in the inertial range (no longer exactly equal to $-5/3 \sim -1.666$, but with a small negative correction amounting for instance to $-\mu/9 \sim -0.022$ after the Kolmogorov–Oboukhov log-normal model [8] and $-\mu/3 \sim -0.066$ after Frisch et al.'s β model [1]), and then roll-off at a still faster rate when the spectral energy flux is progressively depleted by viscosity.

In the energy-containing range, at wave numbers below the inertial range, the picture is obviously much less clear, since the isotropy and universality concepts used in K 41 are no longer valid. Thus the spectrum depends on the particular flow under consideration (in general inhomogeneous and anisotropic) and cannot be ruled by a general theory. For the most frequent situations of turbulent shear flows not far from equilibrium (i.e. when production and dissipation of turbulent kinetic energy are approximately in balance), existing models lead to generalizations of the dynamical spectral equation containing in particular a positive production term (see Hinze [7], Tennekes and Lumley [3]). As a consequence, the predicted spectral exponents are always smaller than $-5/3$ in the production subrange. This can be viewed as a combination of the progressive building-up of the spectral flux of energy $S(k)$ up to its limit value ε when production proceeds, together with the natural tendency of nonlinear interactions to establish a cascade spectrum as $\alpha\varepsilon^{2/3}k^{-5/3}$ as soon as production ceases.

One is thus finally led to the kind of spectral model described in Chapter 8 of Tennekes and Lumley, with a $k^{-5/3}$ inertial domain extending from about $k_l = 10l^{-1}$ to $k_\eta = 0.25\eta^{-1}$. Its width depends on the ratio of the macroscale, l, and the micro (Kolmogorov) scale, η, which is known [3,7] to be given as a function of the turbulence micro (Taylor) scale Reynolds number, $R_\lambda = u\lambda/\nu$, by:

$$l/\eta = \tilde{l} \approx 0.13R_\lambda^{3/2}. \tag{8}$$

Now, the only spectral functions directly measurable in experiments are the longitudinal one-dimensional spectra, most frequently for the longitudinal velocity component, related to $E(k)$ in the isotropic case by:

$$E_{11}^1(k_1) = \int_{k_1}^\infty \frac{E(k)}{k}\left[1 - \frac{k_1^2}{k^2}\right] dk, \tag{9}$$

which leads, for a sufficiently wide inertial subrange, to the well-known expression:

$$E_{11}^1(k_1) = \frac{18}{55}\alpha\varepsilon^{2/3}k_1^{-5/3}, \quad \text{or} \quad \widetilde{E}_{11}^1(\tilde{k}_1) = \frac{18}{55}\alpha\tilde{k}_1^{-5/3}. \tag{10}$$

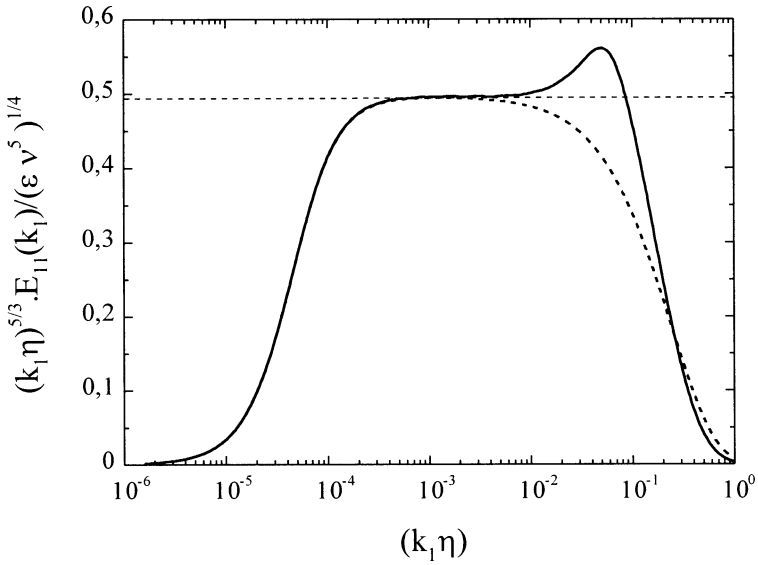

Figure 1. The compensated longitudinal one-dimensional spectrum: (- - - -) after the traditional picture, (——) from experiments, with the bump.

Finally, when plotting a "compensated longitudinal one-dimensional spectrum", namely the product $E_{11}^1(k_1)k_1^{+5/3}$, as a function of k_1, one can expect to get, for a high Reynolds number turbulence, a horizontal inertial-range plateau at the level $\alpha_1\varepsilon^{2/3}$ (with $\alpha_1 = (18/55)\alpha \sim 0.5$). The compensated spectrum should decrease smoothly on both ends of this plateau, the limits of which are lowered by aliasing effects [3,7] at $k_{1l} \sim 2l^{-1}$ and $k_{1\eta} \sim 0.05\eta^{-1}$, as sketched in *figure 1*, dotted line. Soon after the first experimental verifications of the consequences of K 41 (see [7,8]), such compensated spectral plots began to be used as a routine practical method to determine the rate of dissipation, ε. Aside from general purpose practice (Bradshaw [9]), this was commonly applied by micrometeorologists to the measurement, via the constant-flux surface-layer expression, $\varepsilon = U^{*3}/\kappa z$ (eventually corrected for stratification effects), of the atmospheric surface stress, $\tau_0 = \rho U^{*2}$. Known as the "inertial dissipation technique", the method became a favourite for the determination of the momentum flux from the atmosphere to the ocean because it was believed that measurements of high-frequency inertial turbulent eddies would be little affected by the low-frequency effects of the wave and platform motions which disturb the classical $u'w'$ covariance technique (Dreyer [10], Champagne et al. [11]).

3. Early data and discussions about a pre-dissipative spectral bump

People working with such compensated spectral plots, or with plots of $\widetilde{E}_{11}^1(\tilde{k}_1)\tilde{k}_1^{+5/3}$, for determining the Kolmogorov constant α in cases when ε has been otherwise measured, have been the first to notice a systematic difference between their experimental results and the above picture. When using a linear vertical scale, a small but significant 'bump' becomes visible over the range $\tilde{k}_1 \sim 0.01$–0.1 with respect to the plateau level at lower wave numbers. As sketched in *figure 1*, solid line, it appears at a first sight as if the plateau extended up to $k_1 \sim 0.1\eta^{-1}$ together with some uncertainty in the determination of the spectral levels between $0.001\eta^{-1}$ and $0.1\eta^{-1}$. Consequently, the spectral changes associated with this bump are quite easily missed when one uses the usual plot of $\log[E_{11}^1(k_1)]$ versus $\log(k_1)$, but they can however be found by careful inspection. This is manifest for example in Pond et al.'s [12] early results and comments.

Some of the experimental evidence [13,14] for the presence of the bump was supplemented and discussed by Mestayer [15–17] who tried to describe its evolution with the Reynolds number, and realized that its amplitude should be more pronounced for the spectral function $E(k)$ than for its measurable one-dimensional counterpart $E_{11}^1(k_1)$. As in the previous cases, his study raises two types of problems:

– The first one is related to the considerable experimental difficulties encountered in the exploration of the large wave number range in high Reynolds number turbulence. A number of factors act in such a way as to decrease the measured spectral levels: spatial averaging effects along the hot-wire length, insufficient frequency response of the anemometer circuits, excessive attenuation by anti-aliasing filters. On the other hand, other factors increase these levels: spectral 'leakage' from the low wave number strongly energetic range, deviations from Taylor's hypothesis in high intensity turbulent flows, electronic noise, nonlinearity and thermal contamination of the hot-wire response. Techniques can be applied (see [12–17]) to limit and/or correct these detrimental effects, but they necessarily involve assumptions or approximations so that their results always present some uncertainty, as can be ascertained from the notable differences between dissipation spectra obtained from different experiments at neighbouring Reynolds numbers. It is thus clear that any error in the handling of these attenuating and amplifying factors can lead to bump suppression or exaggeration.
– The other kind of difficulty, of much more fundamental importance, stems from the fact that the compensated spectral plateau observed at sufficiently high R_λ below $k_1 \sim 0.01\eta^{-1}$ generally extends down to wave numbers for which, even when taking into account aliasing by one-dimensional spectral representations, local isotropy cannot be expected and its experimental checks indeed fail.

Thus, in addition to large experimental uncertainties, serious doubts could be raised about the significance of this plateau with respect to the results of the K 41 theory. Indication that the plateau and the bump are actually present in the case of locally isotropic turbulence first came from the development of sophisticated spectral closure methods such as the Eddy-Damped-Quasi-Normal-Markovianised, or EDQNM, approximation (see [18–20]). This was particularly clear in André and Lesieur's [18] results. Herring et al. [20] and Mestayer, Chollet and Lesieur [21] identified the origin of the bump as a lack of erosion of the spectra by the elongated non-local triad interactions (i.e. those with $k \ll p \sim q$) when approaching the viscous cut-off. The bump also arose in semi-empirical spectral closures intended to improve the simple Corrsin–Pao model. Developed to take into account the uniform straining process in the dissipative range, Lin's 1972 model [5] logically led to the emergence of a k^{-1} pre-dissipative contribution (see also Rey et al. [22]). The same is true for the models proposed by Hill [23] for the scalar spectrum, when they are utilized for the velocity spectrum [24] by making the Prandtl number equal to unity.

4. Further evidence concerning the bump

From then until the present, an increasing number of independent confirmations of the existence and origin of the bump/plateau combination have appeared in the literature. They stem from entirely different approaches:

4.1. Experimental studies

Experimental studies of very high Reynolds number turbulence in the NASA Ames [25,26] ($R_\lambda \sim 500$–1500) and ONERA Modane [27] ($R_\lambda \sim 1700$–3100) large industrial wind-tunnels. Both exhibit a saddle-type behaviour for the compensated one-dimensional spectra. This is especially clear for the NASA data, a sample of which is shown on *figure 2*, which display a transverse spectral bump more accentuated than the longitudinal one, as can be expected from the different projection operators involved [3]. The existence of a bump, depictable

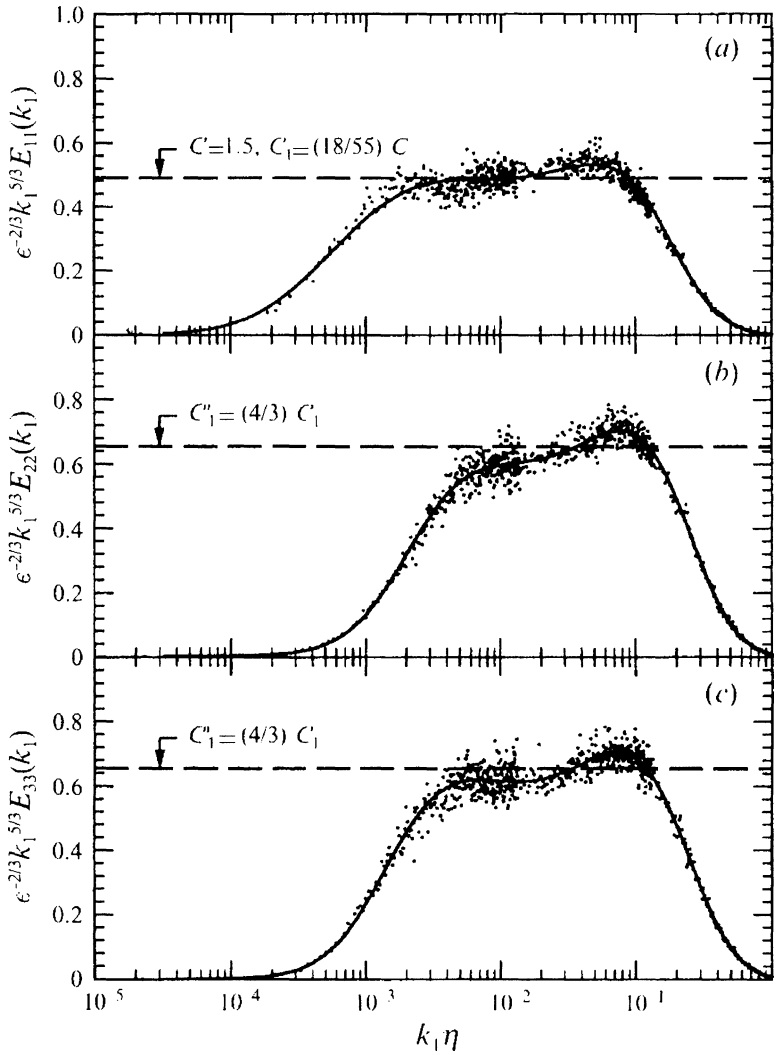

Figure 2. High Reynolds number experimental data from Saddoughi and Veeravalli [25] showing the bumps in longitudinal and transverse compensated spectra (reproduced with permission of Cambridge University Press).

as the emergence of a k^{-1} contribution, is also evident in the 'universal' spectral curve constructed by She and Jackson [28] from experimental data collected by Gagne and Castaing [29].

4.2. Direct numerical simulations

Direct numerical simulations of the small scales of three-dimensional isotropic homogeneous turbulence. Kerr [30,31] found and discussed an accentuated bump at $R_\lambda \sim 80$. Pre-dissipative bumps also appear in Kida and Murakami [32] and Vincent and Meneguzzi [33] and can be discerned in the log–log plots of Sanada [34] at $R_\lambda \sim 100$–180. She et al.'s [35] study also confirms the conclusions of [28] and the existence of a bump. Yeung and Zhou [36] interpret the results of their most recent simulations at R_λ up to 240 as presenting bumps in 3D and 1D spectra. The numerical resolution of a three-dimensional 'Kolmogorov flow' with hyperviscosity for an equivalent R_λ of the order of 1000 by Borue and Orszag [37] also deserves a special mention here. It displays

an exaggerated pre-dissipative bump, as can be expected (see [38]) from to the faster-than-normal hyperviscous energy destruction. Using a reduced wave vector set approximation, Grossman and Lohse [39,40] have been able to extend simulation Reynolds numbers to extremely large values, $R_\lambda \sim 45000$. Their universal spectrum shows clear evidence of a bump, even stronger than in experimental data [28].

4.3. Analytical turbulence closures

Both Qian's [41] variational approach and Yakhot and Zakharov's [42] Clebsch formulation lead to the prediction that the $k^{-5/3}$ inertial law has to be supplemented by a k^{-1} term leading to the appearance of a bump (the analogy with the large viscous-convective k^{-1} bump in scalar spectra had been noted in several of the above references). Falkovich [38] gave a clear physical description and a further theoretical proof of the bump effect, which he befittingly named "bottleneck phenomenon".

4.4. A new complex spectral representation

This was obtained by Sirovich et al. [43] and Lohse and Müller-Groeling [44,45] from the Fourier transform of the interpolation expression for the second-order structure function due to Batchelor [46]. This expression has been shown to provide an excellent fit to Benzi et al.'s [47] data and it can be deduced from the classical [1,8] Kolmogorov equation for the third-order longitudinal structure function:

$$\langle [\Delta u(r)]^3 \rangle = -\frac{4}{5}\varepsilon r + 6\nu d\langle [\Delta u(r)]^2 \rangle / dr. \tag{11}$$

This representation provides clear evidence of the pre-dissipative bump, the extent and significance of which are discussed at length in [44,45].

5. Final comments

We can in conclusion make the following observations:

5.1. Pre-dissipative bump

The existence of a pre-dissipative bump in compensated high-Reynolds number turbulence spectra has now been experimentally, numerically and theoretically demonstrated beyond doubt. So, the classical picture of a $k^{-5/3}$ cascade just depleted by viscous dissipation has to be modified. This observation has only recently emerged in some review papers (Sreenivasan [4], Sreenivasan and Antonia [48]) but, to the best of our knowledge, did not find its way in any of the published monographs on turbulence until recently. This should be changed in the future, to terminate the kind of cultural reluctance against the existence of bumps of which Saddoughi and Veeravalli's [25] statement: "we believe that they are real" gives a typical example.

5.2. Physical origin of the bump

The physical origin of the bump is now fairly well understood (see [4,20,21,38,44,45,48]). The energy flux as given by (6) remains approximately constant until wave numbers of the order of $\tilde{k} \approx 0.1$ when the direct effect of viscous dissipation begins to be felt. Afterwards, the Fourier component amplitude quickly decreases

because of viscous damping. For wave numbers slightly below $\tilde{k} \approx 0.1$, a significant part of the energy flux to higher wave numbers results from elongated non local interactions, and consequently involves triads the long legs of which $p \sim q \gg k$ have been strongly damped. Thus, an energy pileup mechanism appears, which is a 'bottleneck phenomenon' at wave numbers which are still not appreciably depleted by viscosity.

Different data and arguments (see [19,25,44,45]) indicate a saddle-type behaviour of compensated spectra, associated with the existence of another bump at the large-scale end of the inertial plateau. The above reasoning can indeed be extended [44,45] to the consideration of a conserved energy flux, together with triads involving wave numbers of reduced amplitude because of the finite flow size. There are however other problems, associated with anisotropic turbulence production in real-world turbulence and with artificial low-wavenumber forcing in numerical simulations, that prescribe caution in the use of such results.

5.3. Range of application

It has to be stressed that the existence of a pre-dissipative bump in no way contradicts K 41, since its shape appears to be universal as given by (1). The theory indeed establishes that, when the Reynolds number is sufficiently large, there exists a purely inertial, i.e. not directly affected by viscosity, subrange of wave numbers in which (1) can be replaced by (2). However, it does not stipulate how far this subrange extends. The above traditional picture more or less implicitly assumes it goes up to the wave number k_m where the spectral flux begins to be significantly depleted by viscosity, i.e. the ratio $\int_0^{k_m} k^2 E(k)\, dk / \int_0^{\infty} k^2 E(k)\, dk$ ceases to be negligible. In other words, the inertial subrange should end when the dissipative subrange starts. It is now clear that the nonlinear mechanism just described simply extends the range where $E(k)$ is affected by viscosity down to wave numbers well (approximately one decade) below k_m. The bump region can thus be appropriately described in K 41 terms as an "inertio-viscous subrange" separating the "inertial subrange" from the "dissipative subrange".

5.4. Intermittency effects

The very important matter of the consequences of the bump with regard to intermittency effects [1,8] now arises. The reason for which the small negative correction in the second-order inertial spectral slope predicted by K 62 and its successors has not been seen in spectral measurements can obviously be found in the larger offsetting bump influence. One can however note that bumps are in general more visible in wind-tunnels and forced simulations than in geophysical flows: this could be imputed to a stronger large-scale intermittency of the latter which should better counterbalance the energy pileup.

As far as higher-order spectra and structure functions are concerned, one can logically expect that the relative increase in the amplitude of Fourier modes in the inertio-viscous subrange will reflect itself in the local and average scaling exponents. This point has been emphasized by Falkovich [38], and studied in some detail by Grossman and Lohse [39,40]. These authors predict bottleneck corrections growing with the order m of the structure function and stress that the corresponding decrease in the apparent inertial subrange scaling exponents for $m > 3$ can very well be wrongly interpreted as an intermittency correction *a la K 62*. This may require a re-examination of the conclusions drawn from direct structure function slope determinations at laboratory Reynolds numbers (Mestayer [15–17], Anselmet et al. [49]) about the relative merits of different intermittency models [1]. Methods such as those proposed by Stolovotzky et al. [50] or Benzi et al. [47] should be used.

Bumps do not necessarily exist in compensated structure-function plots. Indeed, the detailed analytical study by Lohse and Muller-Groeling [44,45], as well as numerical Fourier transformations of the spectral model to be described later, demonstrate that the second-order spectral bump has a significant effect on the shape and local

slope of the corresponding structure function, but not strong enough to result in a real bump. The monotonic behaviour of $\langle(\Delta u(r))^2\rangle$, together with Kolmogorov's equation (11), also rules out the possibility of bumps in third-order structure functions. As a consequence, the pre-dissipative bumps visible in several published sets of measurements are likely to be the consequence of either the experimental difficulties mentioned in Section 3 or deviations from the homogeneity and isotropy assumptions made in the theory (Selaru-Danaila [51]).

6. A new Reynolds-number-dependent spectral model

For the range of values of R_λ (between one hundred and a few hundreds) usually reached in laboratory experiments, the identification of the bump effect is obscured by the shortening or even the disappearance of the inertial plateau. In addition, a complete (i.e. including the energy-containing and dissipation ranges) Reynolds-number-dependent representation for turbulence spectra is frequently needed for many different purposes (for instance evaluation of constants in one-point closures, determination of dissipation rates, and correction for probe averaging in small-scale measurements [52,53]). Starting from generalizations of the Batchelor interpolation formula, Lohse and Muller-Groeling [44,45] have established very complicated analytical expressions for this representation. We have sought a much simpler R_λ dependent equation based upon elementary phenomenological considerations.

Following Helland et al. [54] and others [55,52], we have chosen to represent $E(k)$ in the energy-containing range by the classical interpolation formula due to Von Karman (see [7]) between k^4 at small k and $k^{-5/3}$ at larger k. Using Kolmogorov-scaled variables:

$$\widetilde{E}(\tilde{k}) = \alpha \tilde{k}^4 / \left(\tilde{l}^{-2} + \tilde{k}^2\right)^{17/6}. \tag{12}$$

This expression needs to be combined with a formulation valid up to very large k for the inertial and viscosity-affected ranges. Since Pao's [6] spectrum used by these authors would not work, we have looked for an improved solution of the spectral equation (4). Introducing a dimensionless time scale $\tilde{\tau}(\tilde{k}) = \tau(k)/\varepsilon^{-1/3}k^{-2/3}$, (5) can be written, with small changes in notation:

$$\widetilde{E}(\tilde{k}) = \beta\alpha_1 \tilde{k}^{-5/3} \tilde{\tau}(\tilde{k}) \exp\left(-2\alpha_2 \int_0^{\tilde{k}} \tilde{k}^{1/3} \tilde{\tau}(\tilde{k})\, d\tilde{k}\right). \tag{13}$$

To get the classical expression (2) in the inertial subrange at high Reynolds numbers, we need to have $\beta\alpha_1 = \alpha$ and $\tilde{\tau}(\tilde{k}) = 1$ at small $\tilde{k}$. We have verified numerically that the addition of a $\tilde{k}^{2/3}$ contribution to the dimensionless time scale, as in Lin [5] and in Hill's [23] model 1, led to the appearance of a bump extending down to wave numbers too small in comparison with experimental data. Working along the same lines as Hill's model 2, we built an expression leading to an hyperbolic tangent shape of the bump in semi-log coordinates, with adjustable amplitude A, transition wave number $\tilde{k}_1$ and width, namely:

$$\tilde{\tau}_1(\tilde{k}) = 1 + A\left[(\tilde{k}/\tilde{k}_1)^n / \left[1 + (\tilde{k}/\tilde{k}_1)^n\right]\right]. \tag{14}$$

At large k, this tends to $1 + A$, so that (13) would follow the 'a la Pao' behaviour in the far dissipative range. This clearly cannot be accepted since theoretical, numerical and experimental studies (recently reviewed by Domaradzki [56] and Nelkin [57]) now agree to a simple exponential roll-off with algebraic prefactor, for the constants a and b of which quite different values have been proposed:

$$\widetilde{E}(\tilde{k}) = Cte\tilde{k}^a \exp(-b\tilde{k}). \tag{15}$$

To get such a behaviour, it is clear from (13) that $\tilde{\tau}(\tilde{k})$ needs to have a $\tilde{k}^{-1/3}$ limit. This will lead to the k^{-2} prefactor advocated by Domaradzki and predicted a long time ago by Dugstad [58]. We thus multiply (14) by another expression with two additional adjustable constants:

$$\tilde{\tau}_2(\tilde{k}) = \left[1 + (\tilde{k}/\tilde{k}_2)^m\right]^{-1/3m}. \tag{16}$$

The complete R_λ-dependent spectral representation thus finally obeys:

$$\widetilde{E}(\tilde{k}) = \beta\alpha_1 \tilde{k}^4 \left(\tilde{l}^{-2} + \tilde{k}^2\right)^{-17/6} \tilde{\tau}(\tilde{k}) \exp\left(-2\alpha_2 \int_0^{\tilde{k}} \tilde{k}^{1/3} \tilde{\tau}(\tilde{k})\, d\tilde{k}\right), \tag{17}$$

with

$$\tilde{\tau}(\tilde{k}) = \left\{1 + A\left[(\tilde{k}/\tilde{k}_1)^n / (1 + (\tilde{k}/\tilde{k}_1)^n)\right]\right\} (1 + (\tilde{k}/\tilde{k}_2)^m)^{-1/3m}.$$

7. Setting the constants in the model

Recourse to experimental data is necessary to assign numerical values to the various constants in (17). This has proven not to be an easy task, since many of the published spectra were either not in a form suitable to our analysis, or did not properly obey the consequences of the above theoretical considerations concerning fully developed turbulence. We have essentially relied upon measurements of one-dimensional longitudinal spectra, requesting them to fulfill the obviously necessary following conditions:

(i) Provide reasonable indications for a locally isotropic behaviour of their small and at least part of their intermediate scales;

(ii) Possess a proper shape at dissipative scales, as close to universal as possible, with a good asymptotic tendency of the dissipation spectrum towards zero at high wave numbers, and an exact verification of the one-dimensional normalization condition:

$$\int_0^\infty \tilde{k}_1^2 \widetilde{E}_{11}^1(\tilde{k}_1)\, d\tilde{k}_1 = 1/15; \tag{18}$$

(iii) Display in the compensated spectrum a bump of close to universal shape and near to the average height, thus excluding apparently underdeveloped as well as overdeveloped cases;

(iv) Display an acceptable behaviour for inertial scales, with adequate values of power-law exponents and Kolmogorov constants at sufficiently large Reynolds numbers, and plausible monotonic changes as a function of the latter parameter.

A rather extensive literature search indeed showed that not much progress had been achieved in the solution of the considerable experimental difficulties mentioned in Section 3 since past careful studies such as Champagne's [14], and that several recently published sets of data failed to pass the above ensemble of tests and hence could not be used. Adopting an admittedly somewhat subjective procedure, we finally decided to determine the constants in our model after two representative series of measurements taken under widely different conditions and obeying particularly well our requirements: some of the very high Reynolds number spectra obtained by Saddoughi and Veeravalli [25], and those obtained at lower Reynolds numbers by Mydlarski and Warhaft [59,60].

Considering the level of the inertial plateau, we took the generally accepted value $\alpha_1 = 1.50$ together with $\beta = 1$ at high Reynolds numbers. The three next constants, $A = 0.57$, $\tilde{k}_1 = 0.07$ and $n = 3$ have been

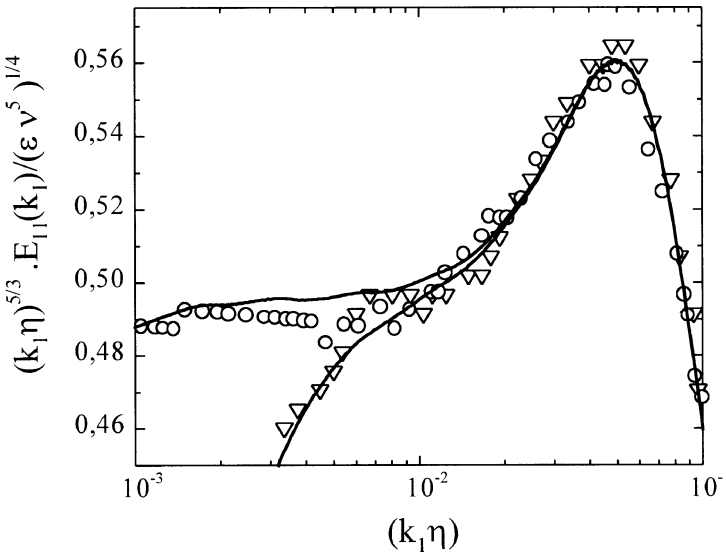

Figure 3. Present results compared with high Reynolds number data around the bump region. (——) Present work; (▽) Mydlarsky and Warhaft [59] for isotropic grid turbulence at $R_\lambda = 373$; (○) Saddoughi and Veeravalli [25] for boundary layer at $R_\lambda = 1450$.

adjusted after the average bump shape observed at two different Reynolds numbers ($R_\lambda = 373$ and 1450) for $\widetilde{E}^1_{11}(\tilde{k}_1)\tilde{k}_1^{+5/3}$, as shown in *figure 3*. For the last constants, since the limit behaviour of (17) is:

$$\widetilde{E}(\tilde{k}) = Cte\tilde{k}^{-2}\exp\left[-\left(2\alpha_2(1+A)\tilde{k}_2^{1/3}\right)\tilde{k}\right], \tag{19}$$

use should be made of experimental determinations of the constant b in equation (15). We need however to take into account that, contrary to the inertial subrange transformation from (2) to (10), a dissipative three-dimensional spectrum of the form (15) does not lead, in locally isotropic turbulence, to a one-dimensional spectrum with the same shape. This point has been sometimes overlooked in the recent literature. It is easily demonstrated from the inverse transformation:

$$\widetilde{E}^1_{11}(\tilde{k}) = C\tilde{k}^a\exp(-b\tilde{k}) \rightarrow$$

$$\widetilde{E}(\tilde{k}) = \frac{\tilde{k}^3}{2}\frac{d}{d\tilde{k}}\left[\frac{1}{\tilde{k}}\frac{d\widetilde{E}^1_{11}(\tilde{k})}{d\tilde{k}}\right] = \frac{C}{2}\tilde{k}^a\left\{b^2\tilde{k}^2 + b(1-2a)\tilde{k} + a(a-2)\right\}\exp(-b\tilde{k}). \tag{20}$$

We finally found by trial and error that the physically plausible value $\tilde{k}_2 = 0.32$ for the transition wave number in (16), together with $m = 4$ for a rapid transition and $\alpha_2 = 1.527$, led to an excellent fit with Saddoughi and Veeravalli's [25] one-dimensional data in the dissipation range, as shown by *figure 4*. At the same time, the normalization condition (18) is found to be verified to better than 1% at high Reynolds numbers.

8. Results and discussion

8.1. Spectral parameterization as a function of R_λ

The influence of the flow Reynolds number upon the spectrum results from the presence of the $\tilde{l}^{-2}$ term in (17). Adopting for the macroscale the definition [3] $l = u^3\varepsilon^{-1}$, it is easily shown that:

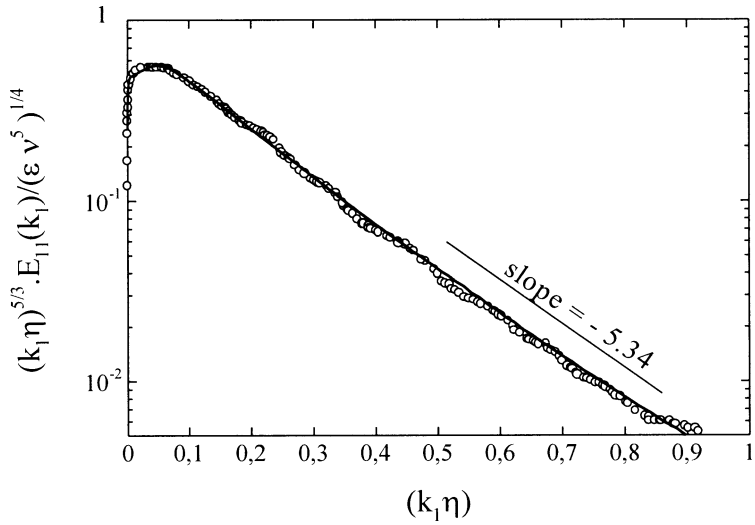

Figure 4. Present work compared with Saddoughi and Veeravalli's [25] data in the dissipation range at $R_\lambda = 600$.

$$\tilde{l} = \frac{l}{\eta} = \left(\frac{2\sqrt{15}}{3} I\right)^{-3/2} R_\lambda^{+3/2} = D R_\lambda^{+3/2}, \tag{21}$$

with $I = \int_0^\infty \tilde{E}(\tilde{k})\, d\tilde{k}$.

At large R_λ, this integral is dominated by the Von Karman contribution and the coefficient D in (8) and (21) equals 0.125. For smaller (i.e. below 100) R_λ, the energy and dissipation ranges overlap and D becomes Reynolds number dependent. Simultaneously, the multiplicative coefficient β in (17) needs to be adjusted to keep (18) true (Pao [6], Driscoll and Kennedy [24]). *Figure 5* displays the computed coupled variations of D and β as functions of R_λ, and thus allows a complete determination of the spectrum as a function of this single parameter.

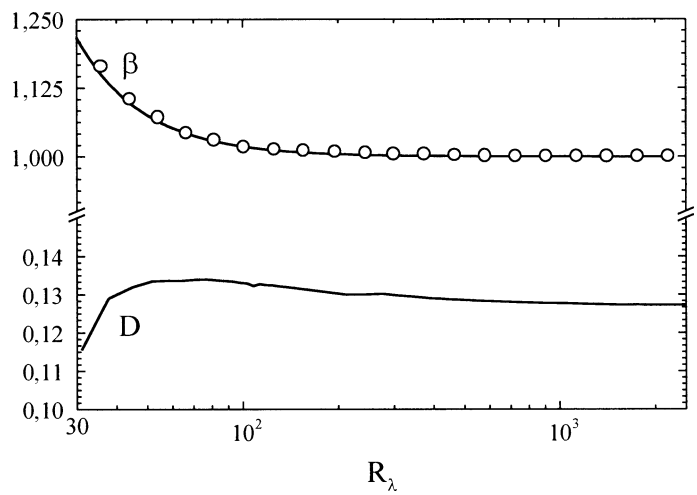

Figure 5. Variation of coefficients D and β with R_λ. ∘ represents the results obtained by Driscoll and Kennedy [24].

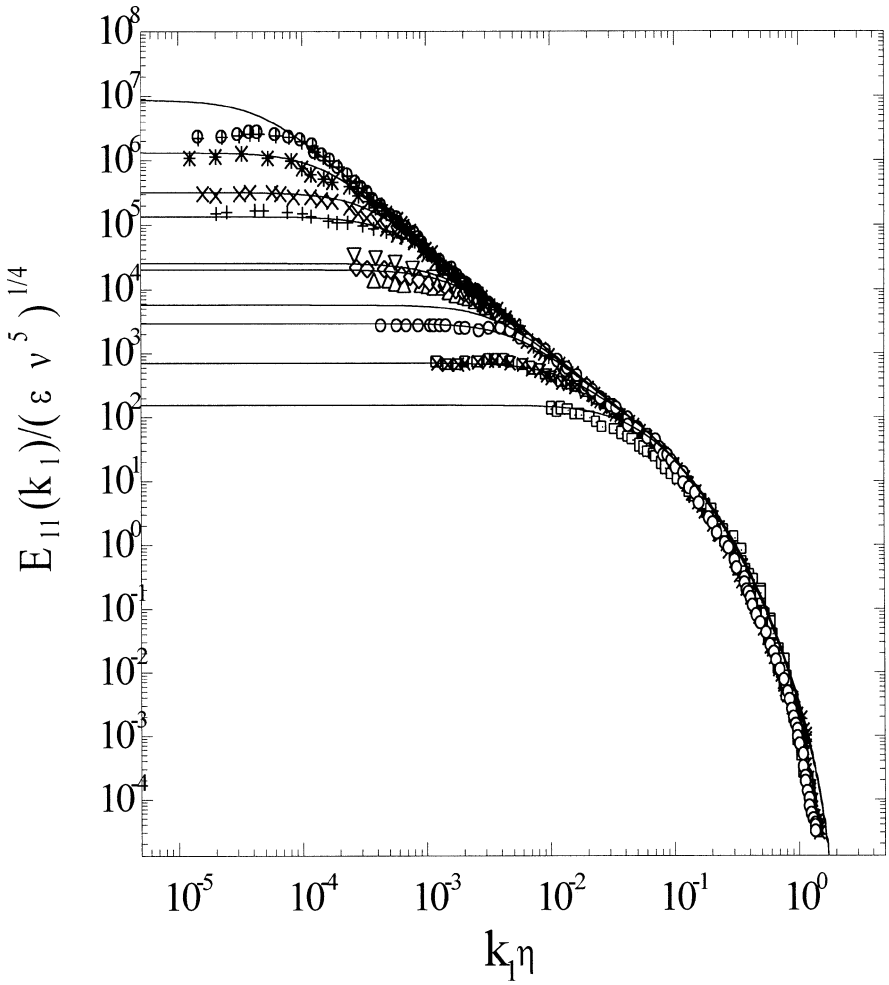

Figure 6. Kolmogorov's universal scaling for one-dimensional longitudinal power spectra. The present results (solid lines) are compared with data from experiments compiled by Chapman with later additions by Saddoughi and Veeravalli [25]. (□) $R_\lambda = 37$ and $R_\lambda = 72$, grid turbulence (Comte-Bellot and Corrsin [61]); (○) $R_\lambda = 130$ homogeneous shear flow (Champagne et al. [62]); (△) $R_\lambda = 170$ pipe flow (Laufer [63]); (◇) $R_\lambda = 282$ boundary layer (Tielman [64]); (▽) $R_\lambda = 308$ wake behind cylinder (Uberoi and Freymuth [65]); (+) $R_\lambda = 600$ boundary layer (Saddoughi and Veeravalli [25]); (×) $R_\lambda = 850$ boundary layer (Coantic and Favre [66]); (∗) $R_\lambda = 1500$ boundary layer (Saddoughi and Veeravalli [25]); (⊕) $R_\lambda = 3180$ return channel (Karyakin et al. [67]).

8.2. Description of the large energy-containing scales

With the aid of the isotropy relation (9), the non-dimensional longitudinal spectrum $\widetilde{E}_{11}^{1}(\tilde{k}_1)$ has then been determined for ten different values of the microscale Reynolds number varying between 37 and 3180. Its low- and medium-frequency behaviour is compared in *figure 6* with the corresponding experimental spectra [61–67] taken from Saddoughi and Veeravalli [25]. In most of the cases, the agreement is quite good and indeed better than what could have been anticipated in view of the rather naive assumptions involved in our computations. This encouraged us to make a test for the R_λ dependence of the constant E in the expression:

$$\varepsilon = Eu'^3/l_{11}, \tag{22}$$

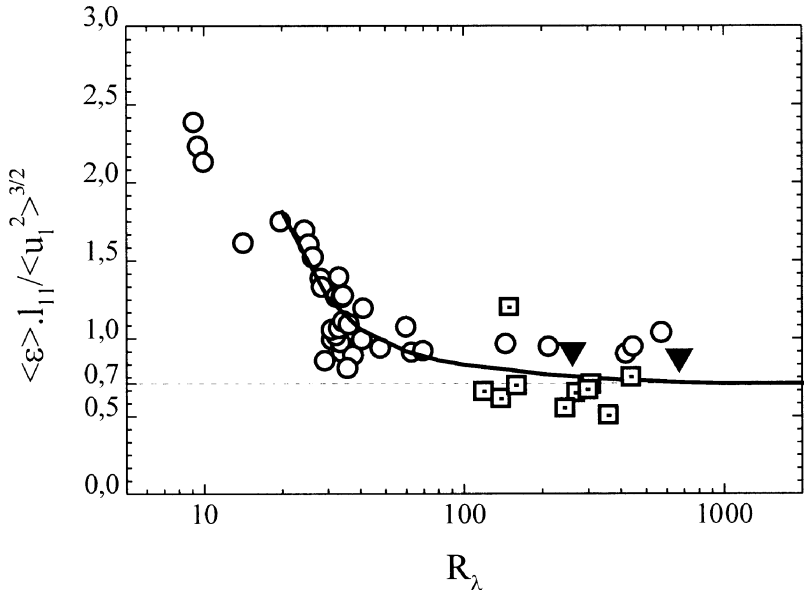

Figure 7. The coefficient $E = \varepsilon l_{11}/u'^3$ as a function of R_λ. (——) Present work; (○) biplane square-mesh grid turbulence [68]; (⊡) homogeneous shear flows [69]; (▼) boundary layer [25].

where l_{11} is the longitudinal macroscale of turbulence. One easily gets:

$$E = \varepsilon l_{11}/u'^3 = \frac{\pi}{2}\int_0^\infty \frac{\tilde{E}(\tilde{k})}{\tilde{k}}\,d\tilde{k}\left[\frac{2}{3}\int_0^\infty \tilde{E}(\tilde{k})\,d\tilde{k}\right]^{-5/2}. \tag{23}$$

The variation predicted by the model is compared in *figure 7* with the experimental data collected by Sreenivasan [68,69] for homogeneous non-sheared and sheared turbulence, plus two additional points determined after Mydlarski and Warhaft [59,60]. The model describes satisfactorily well the general tendency of the rather scattered data, with a high Reynolds number limit $E_\infty \approx 0.71$ as given by the Von Karman spectrum.

8.3. Description of the intermediate inertial scales

In *figure 8*, compensated non-dimensional longitudinal spectra $\tilde{k}_1^{5/3}\tilde{E}_{11}^1(\tilde{k}_1)$ computed with the present representation are compared with several experimental data sets in the range of microscale Reynolds numbers $R_\lambda = 100$–1500. The fit is rather good, and the obvious R_λ dependency is well described by the model.

The apparent variation in the inertial subrange behaviour observed by Mydlarski and Warhaft [59,60] is now easily explained as a simple consequence of the large scale limitation at finite Reynolds numbers. By processing the spectra given by the model in the same way these authors treated their experimental spectra, we get the results shown in *figure 9*. The R_λ shifts of the apparent spectral slope, n_1, and constant, C_1^*, given by the model fit rather nicely the experimentally determined values. One can note here that, using the relationship $R_\lambda \sim Re^{1/2}$, the observed Reynolds number dependency of the spectral slope correction, $\delta n_1 \sim R_\lambda^{-2/3=-0.66}$, corresponds closely to the finite size correction predicted by Grossmann et al. [70], $\delta n_1 \sim Re^{-3/10} \sim R_\lambda^{-0.60}$.

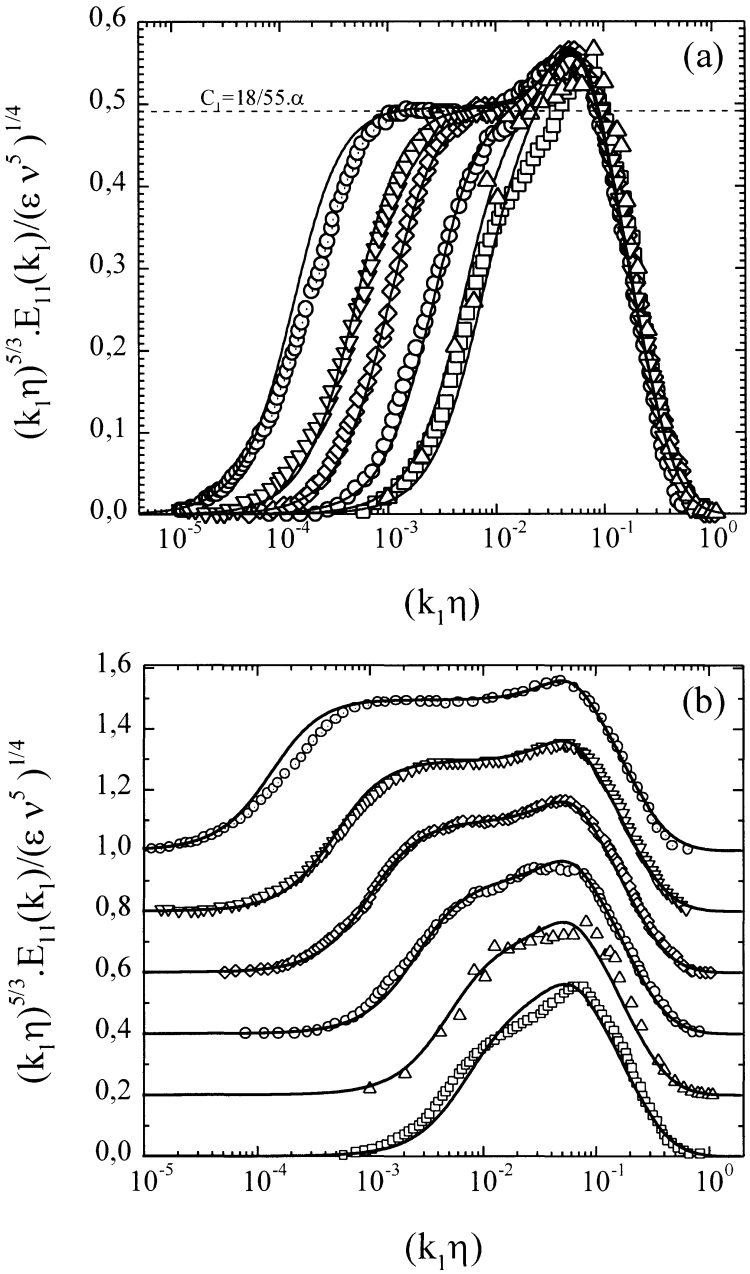

Figure 8. Comparison of model-predicted (solid lines) and experimental compensated non-dimensional longitudinal spectra for $R_\lambda = 99$ (□); 130 (△), 199 (○), 373 (◇), 600 (▽), 1450 (⊙). In (b), the successive curves are shifted upwards by 0.2 for clarity.

8.4. Description of the small dissipative scales

Longitudinal dissipation spectra, $\tilde{k}_1^2\tilde{E}_{11}^1(\tilde{k}_1)$, are shown in *figure 10* for comparison with several sets of experimental data corresponding either to the large ($R_\lambda > 500$) or to the small Reynolds number range. Note that in the latter case it was found necessary to rescale the ordinates of the data points to obtain a better fulfilment of the normalization condition (18). The overall agreement is again rather satisfactory, and the

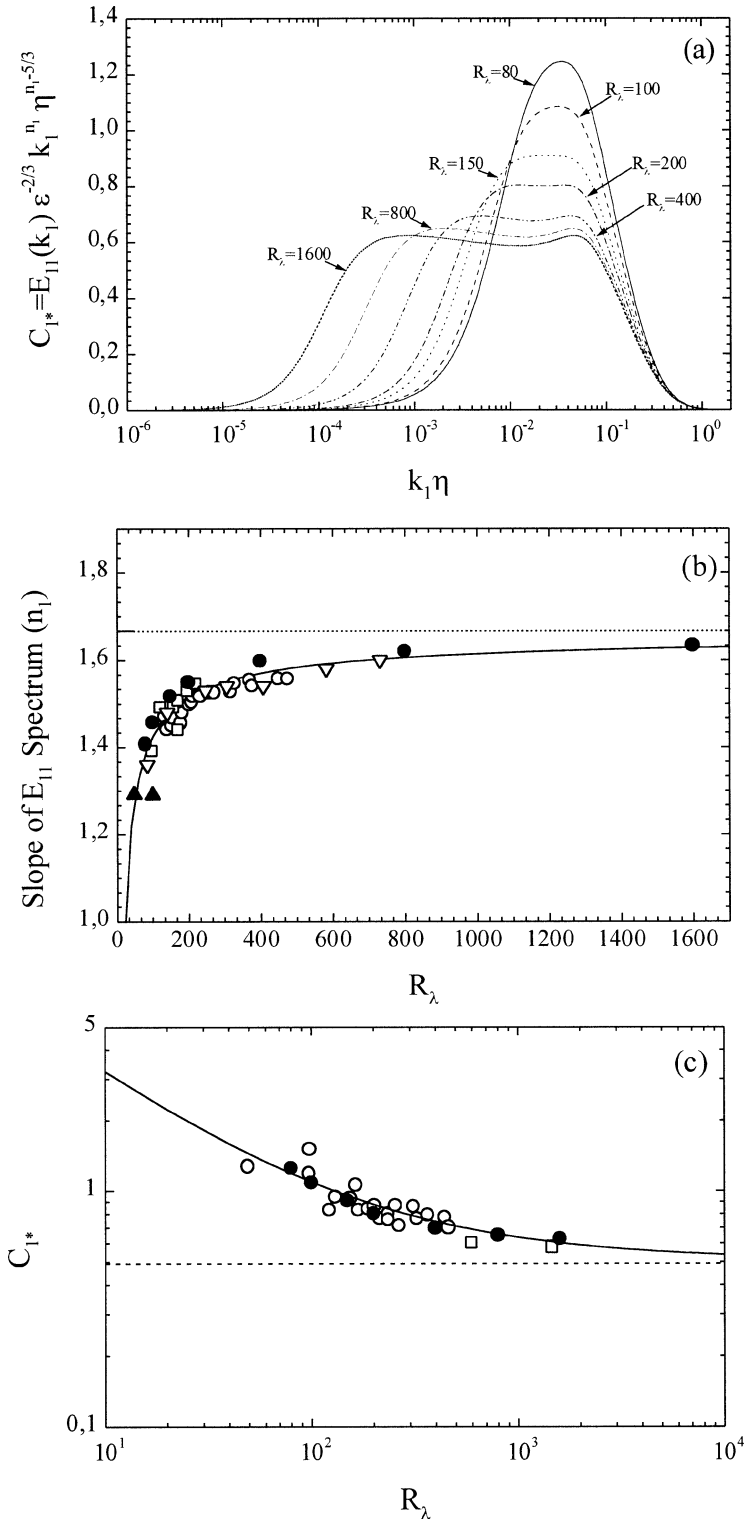

Figure 9. Comparison of the model results with Mydlarski and Warhaft's [59,60] data: (a) optimally compensated model spectra at different R_λ; (b) and (c) corresponding variations of the spectral exponent n_1 and constant C_{1*} (the model results correspond to full circles for (b) and (c)).

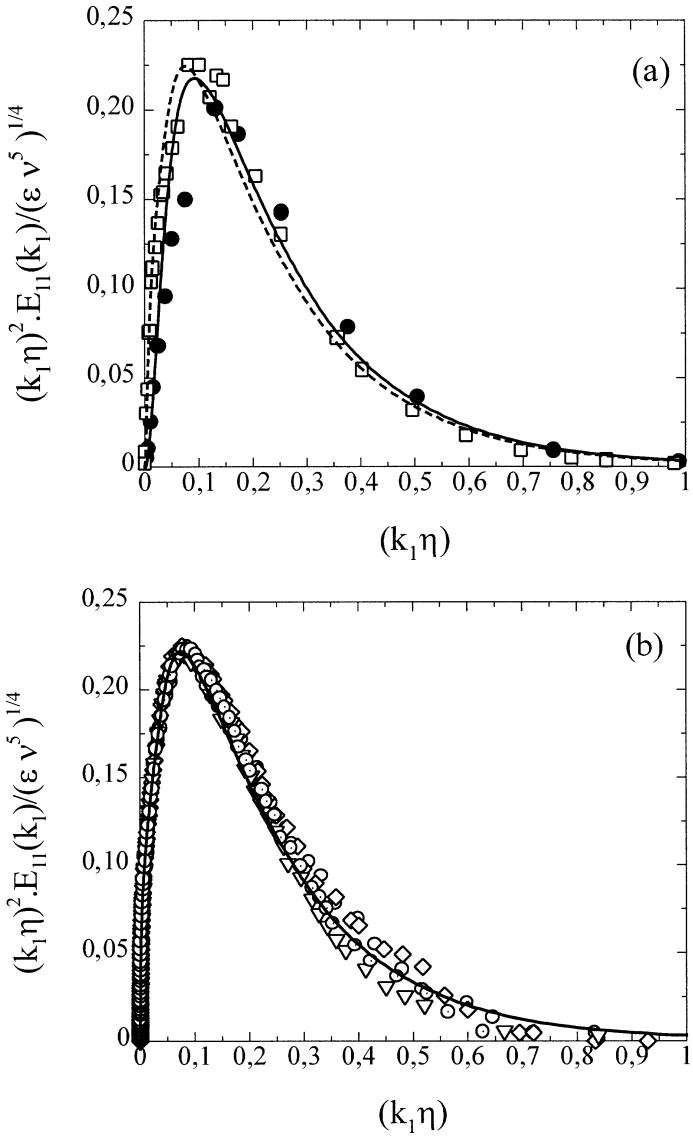

Figure 10. Longitudinal dissipation spectra (a) predictions and data for $R_\lambda = 41$ (——, •) and $R_\lambda = 130$ (——, □); (b) large R_λ prediction and data at $R_\lambda = 199$ (○), 373 (◇), 600 (▽), 1450 (⊙).

changes in the spectral maximum level and position due to large scale limitation at the lowest Reynolds numbers are well captured by the model.

8.5. Skewness factor variations

A sensitive test for global spectral representations is to compare the result from the well known expression (Wyngaard and Tennekes [71]):

$$S\left(\frac{\partial u}{\partial x}\right) = -116\int_0^\infty \tilde{k}^4 \tilde{E}(\tilde{k})\, d\tilde{k}, \tag{24}$$

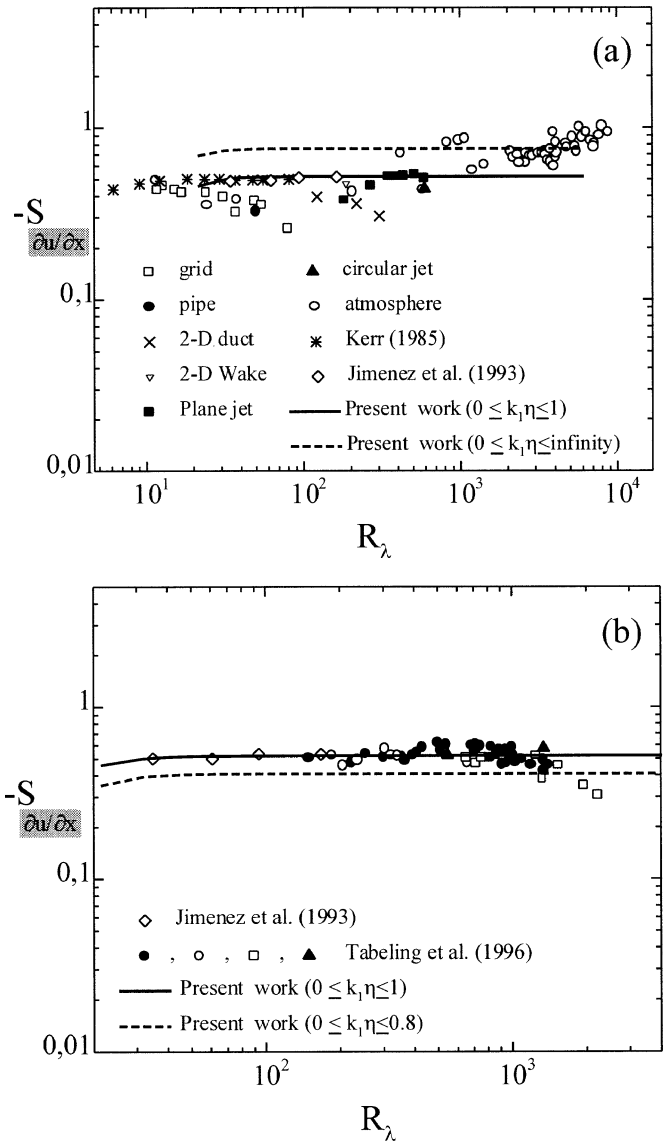

Figure 11. Comparison between computed velocity derivative skewness factors, and (a) the data collected by Sreenivasan and Antonia [48], see also [30,31,76]; (b) the measurements by Tabeling et al. [75], see also [76].

with experimental data for the skewness factor of the longitudinal velocity derivative as a function of R_λ, admitting the high Reynolds number assumption leading to (24) is still valid at the smaller microscale Reynolds numbers under consideration (Smith and Reynolds [72], Manley [73], Sanada [74]). Such a comparison is shown in *figure 11* with respect to (a) the data collected by Sreenivasan and Antonia [48], and (b) the recent measurements of Tabeling et al. [75]. Our results fully confirm Manley's conclusion that the computed skewness factors significantly depend on the effective upper wave number limit used in the above integral to take into account the limited spectral content of the available data. The values we obtain when adopting his average figure $\tilde{k} = 1$ are in quite good agreement with most of the data up to R_λ of the order of 10^3. For still larger microscale Reynolds numbers, at least part of the noted divergence (see [48,75]) between the older atmospheric

skewnesses and the recent laboratory data could be attributed to a lower spectral limitation of the latter ones (see Tabeling et al.'s figure 12). The additional variations found at extremely high R_λ could eventually (see Frisch [1]) be attributed to small-scale spectral modifications due to intermittency effects *a la K 62*, as had been concluded by Champagne [14].

9. Conclusions

The quite varied evidence we have gathered undeniably demonstrates the existence of a pre-dissipative spectral 'bump' in high Reynolds number compensated turbulence spectra, as a consequence of an energy pileup mechanism leading to the presence of an 'inertio-viscous subrange' between the purely inertial and dissipative subranges.

The fact that this bump is not always visible, or on the contrary appears as exaggerated in some experimental data, could be attributed to three categories of reasons:

(i) The considerable experimental difficulties in obtaining accurate unbiased data associated with the small scales of high Reynolds number turbulence;

(ii) The fact that, under the conditions generally encountered in laboratory experiments, the bump effect is necessarily confused with the consequences of the limitation in Reynolds number. One of the main interests of our proposed R_λ-dependent simple spectral model is to disentangle the two processes and to provide an easy explanation for the changes with Reynolds number observed in the supposedly purely inertial subrange behaviour;

(iii) The effects of intermittency, particularly in extremely large Reynolds number geophysical flows. Since these effects tend to increase the negative second-order spectral exponent, while the energy pile-up mechanism acts in the opposite direction, the final result will depend on their relative importance. As already noted, this can explain well why the bumps are in general more clearly seen in moderate to high Reynolds number numerical simulations and laboratory experiments than in very high Reynolds number geophysical flows (see Mestayer [15–17], Sreenivasan [4]). One can also mention that part of the scatter observed between data taken at nearby microscale Reynolds numbers could be attributed to the differences in the large-scale flow structures involved, leading to differences in the levels of small-scale intermittency.

Our simple spectral model does not take into account the latter, uses an admittedly oversimplified representation of the large scales, and will certainly fail in cases of strongly sheared turbulence. It is however found to work rather nicely in various situations covering a reasonably wide range of Reynolds numbers. It could be improved if more reliable spectral data with less scatter were available. Carefully performed measurements using the same set of instruments and methods in turbulent flows of varied geometries, sizes and velocities are obviously still needed today.

Acknowledgements

Supports of Electricité de France under contract 2M9365/AEE 2256 and of G.I.E. PSA Peugeot–Citroën under contract CNRS/74077 are gratefully acknowledged. Thanks are also due to F. Anselmet for his comments on an early version of this paper, and to M. Mydlarski and Z. Warhaft for making available some of their numerical data sets.

References

[1] Frisch U., Turbulence: The Legacy of A.N. Kolmogorov, Cambridge University Press, Cambridge, 1995.
[2] Lesieur M., Turbulence in Fluids, Kluwer Academic Publishers, Dordrecht, 1990.
[3] Tennekes H., Lumley J.L., A First Course in Turbulence, MIT Press, Cambridge, MA, 1972.
[4] Sreenivasan K.R., On the universality of the Kolmogorov constant, Phys. Fluids 7 (1995) 2778–2784.
[5] Lin J.T., Velocity spectrum of locally isotropic turbulence in the inertial and dissipation ranges, Phys. Fluids 15 (1972) 205–207.
[6] Pao Y.H., Structure of turbulent velocity and scalar fields at large wave-numbers, Phys. Fluids 8 (1965) 1063–1075.
[7] Hinze J.O., Turbulence, MacGraw-Hill, New York, 1975.
[8] Monin A.S., Yaglom A.M., Statistical Fluid Mechanics, Vol. 2, MIT Press, Cambridge, MA, 1975.
[9] Bradshaw P., Conditions for the existence of an inertial subrange in turbulent flow, N.P.L. Aero Report 1220, Aero. Res. Counc. R. & M. 28664, London, 1967.
[10] Dreyer G.F., Comparison of momentum, sensible and latent heat fluxes determined over the ocean by the direct covariance, inertial and dissipation techniques, Ph.D. Thesis, Univ. of California, San Diego, 1974.
[11] Champagne F.H., Friehe C.A., La Rue J.C., Wyngaard J.C., Flux measurements, flux-estimation techniques, and fine-scale turbulence measurements in the unstable surface layer over land, J. Atmos. Sci. 34 (1977) 515–530.
[12] Pond S., Stewart R.W., Burling R.W., Turbulence spectra in the wind over waves, J. Atmos. Sci. 20 (1963) 319–324.
[13] Williams R.M., Paulson C.A., Microscale temperature and velocity spectra in the atmospheric boundary layer, J. Fluid Mech. 83 (1977) 547–567.
[14] Champagne F.H., The fine-scale structure of the turbulent velocity field, J. Fluid Mech. 86 (1978) 67–108.
[15] Mestayer P., De la structure fine des champs turbulents dynamiques et thermiques pleinement développés en couches limites, Thèse Doct. es Sci., Univ. Aix-Marseille II, 1980.
[16] Mestayer P., De la structure fine des champs turbulents dynamiques et thermiques pleinement développés en couches limites, Bulletin Direction Etudes et Recherches, Electricite de France, Paris, A 4, 1981.
[17] Mestayer P., Local isotropy and anisotropy in a high-Reynolds-number turbulent boundary layer, J. Fluid Mech. 125 (1982) 475–503.
[18] André J.C., Lesieur M., Influence of helicity on the evolution of isotropic turbulence at high Reynolds number, J. Fluid Mech. 81 (1977) 187–207.
[19] Chollet J.P., Lesieur M., Parameterization of small scales of three-dimensional isotropic turbulence utilizing spectral closures, J. Atmos. Sci. 38 (1981) 2747–2757.
[20] Herring J.R., Schertzer D., Lesieur M., Newman G.R., Chollet J.P., Larcheveque M., A comparative assessment of spectral closures as applied to passive scalar diffusion, J. Fluid Mech. 124 (1982) 411–438.
[21] Mestayer P., Chollet J.P., Lesieur M., Inertial subrange and velocity and scalar variance spectra in high Reynolds number three-dimensional turbulence, in: Tatsumi T. (Ed.), Turbulence and Chaotic Phenomena in Fluids, Elsevier Science Publishers, 1984, pp. 285–288.
[22] Rey C., Schon J.P., Mathieu J., Modèle de transfert spectral pour les petites structures de champs turbulents scalaires et cinématiques, C. R. Acad. Sci. II B 283 (1976) 293–296.
[23] Hill R.J., Models of the scalar spectrum for turbulent advection, J. Fluid Mech. 88 (1978) 541–562.
[24] Driscoll R.J., Kennedy L.A., A model for the turbulent energy spectrum, Phys. Fluids 26 (1983) 1228–1233.
[25] Saddoughi S.G., Veeravalli S.V., Local isotropy in turbulent boundary layers at high Reynolds number, J. Fluid Mech. 268 (1994) 333–372.
[26] Saddoughi S.G., Local isotropy in complex turbulent boundary layers at high Reynolds number, J. Fluid Mech. 348 (1997) 201–245.
[27] Marchand M., Propriétés statistiques des petites structures dans les écoulements turbulents: influence du nombre de Reynolds sur l'intermittence, Thèse Doct., Inst. Nat. Polytech. Grenoble, 1994.
[28] She Z.S., Jackson E., On the universal form of energy spectra in fully developed turbulence, Phys. Fluids A 5 (1993) 1526–1528.
[29] Gagne Y., Castaing B., Une représentation universelle sans invariance globale d'échelle des spectres d'énergie en turbulence développée, C. R. Acad. Sci. II 312 (1991) 441–445.
[30] Kerr R.M., Higher-order derivative correlations and the alignment of small-scale structures in isotropic numerical turbulence, J. Fluid Mech. 153 (1985) 31–58.
[31] Kerr R.M., Vorticity, scalar and transfer spectra in numerical turbulence, J. Fluid Mech. 211 (1990) 309–332.
[32] Kida S., Murakami Y., Kolmogorov similarity in freely decaying turbulence, Phys. Fluids 30 (1987) 2030–2039.
[33] Vincent A., Meneguzzi M., The spatial structure and statistical properties of homogeneous turbulence, J. Fluid Mech. 225 (1991) 1–25.
[34] Sanada T., Cluster statistics of homogeneous fluid turbulence, Phys. Rev. A 44 (1991) 6480–6489.
[35] She Z.S., Chen S., Doolen G., Kraichnan R.H., Orszag S.A., Reynolds number dependence of isotropic Navier–Stokes turbulence, Phys. Rev. Lett. 70 (1993) 3251–3254.
[36] Yeung P.K., Zhou Y., Universality of the Kolmogorov constant in numerical simulations of turbulence, Phys. Rev. E 56 (1997) 1746–1752.
[37] Borue V., Orszag S.A., Numerical study of three-dimensional Kolmogorov flow at high Reynolds numbers, J. Fluid Mech. 306 (1996) 293–323.
[38] Falkovich G., Bottleneck phenomenon in developed turbulence, Phys. Fluids 6 (1994) 1411–1414.
[39] Grossmann S., Lohse D., Universality in fully developed turbulence, Phys. Rev. E 50 (1994) 2784–2789.
[40] Grossmann S., Lohse D., Scale resolved intermittency in turbulence, Phys. Fluids 6 (1994) 611–617.
[41] Qian J., Universal equilibrium range of turbulence, Phys. Fluids 27 (1984) 2229–2233.

[42] Yakhot V., Zakharov V., Hidden conservation laws in hydrodynamics; energy and dissipation rate fluctuation spectra in strong turbulence, Physica D 64 (1993) 379–394.
[43] Sirovich L., Smith L., Yakhot V., Energy spectrum of homogeneous and isotropic turbulence in far dissipation range, Phys. Rev. Lett. 72 (1994) 344–347.
[44] Lohse D., Müller-Groeling A., Bottleneck effects in turbulence: scaling phenomena in r versus p space, Phys. Rev. Lett. 74 (1995) 1747–1750.
[45] Lohse D., Müller-Groeling A., Anisotropy and scaling corrections in turbulence, Phys. Rev. E 54 (1996) 395–405.
[46] Batchelor G.K., Pressure fluctuations in isotropic turbulence, Proc. Cambridge Philos. Soc. 47 (1951) 359–374.
[47] Benzi R., Ciliberto S., Baudet C., Chavarria G.R., On the scaling of three-dimensional homogeneous and isotropic turbulence, Physica D 80 (1995) 385–398.
[48] Sreenivasan K.R., Antonia R.A., The phenomenology of small-scale turbulence, Annu. Rev. Fluid Mech. 29 (1997) 435–472.
[49] Anselmet F., Gagne Y., Hopfinger E.J., Antonia R.A., High-order velocity structure functions in turbulent shear flow, J. Fluid Mech. 140 (1984) 63–89.
[50] Stolovitzky G., Sreenivasan K.R., Juneja A., Scaling functions and scaling exponents in turbulence, Phys. Rev. E 48 (1993) 3217–3220.
[51] Selaru-Danaila L., Influence des grandes échelles sur le mélange turbulent d'un scalaire passif, Thèse Doct., Univ. Aix-Marseille II, 1998.
[52] Ewing D., Hussein H.J., George W.K., Spatial resolution of parallel hot-wire probes for derivative measurements, Exp. Therm. Fluid Sci. 11 (1995) 155–173.
[53] Zhu Y., Antonia R.A., The spatial resolution of hot-wire arrays for the measurement of small-scale turbulence, Meas. Sci. Technol. 7 (1996) 1349–1359.
[54] Helland K.N., Van Atta C.W., Stegen G.R., Spectral energy transfer in high Reynolds number turbulence, J. Fluid Mech. 79 (1977) 337–359.
[55] Rey C., Effets du nombre de Prandtl, de la gravité et de la rugosité sur les spectres de turbulence cinématique et scalaire, Thèse Doct. es Sci., Univ. Lyon 1, 1977.
[56] Domaradzki J.A., Nonlocal triad interactions and the dissipation range of isotropic turbulence, Phys. Fluids A 4 (1992) 2037–2045.
[57] Nelkin M., Universality and scaling in fully developed turbulence, Adv. Phys. 43 (1994) 143–181.
[58] Dugstad I., A hypothesis about the energy transfer in isotropic turbulence, Meteorologiske Annaler 4 (1962) 441–462.
[59] Mydlarski M., Warhaft Z., On the onset of high-Reynolds number grid-generated wind tunnel turbulence, J. Fluid Mech. 320 (1996) 331–368.
[60] Mydlarski M., Warhaft Z., Passive scalar statistics in high-Péclet-number grid turbulence, J. Fluid Mech. 358 (1998) 135–175.
[61] Comte-Bellot G., Corrsin S., Simple Eulerian time correlation of full and narrow-band velocity signals in grid-generated 'isotropic' turbulence, J. Fluid Mech. 48 (1971) 273–337.
[62] Champagne F.H., Harris V.G., Corrsin S., Experiments on nearly homogeneous turbulent shear flow, J. Fluid Mech. 41 (1970) 81–139.
[63] Laufer J., The structure of turbulence in fully developed pipe flow, NACA Rep. 1174, 1954.
[64] Tieleman H.W., Viscous region of turbulent boundary layer, Colorado State Univ. Rep. CER, 67–68 HWT21, 1967.
[65] Uberoi M.S., Freymuth P., Spectra of turbulence in wakes behind circular cylinders, Phys. Fluids 12 (1969) 1359–1363.
[66] Coantic M., Favre A., Activities in, and preliminary results of, air–sea interactions research at I.M.S.T., Adv. Geophys. 18A (1974) 391–405.
[67] Karyakin M.Y., Kuznetsov V.R., Praskovsky A.A., Izv. Adad. Nauk SSSR, Mech. Zhidk. i Gaza 5 (1991) 51–59.
[68] Sreenivasan K.R., On the scaling of the energy dissipation rate, Phys. Fluids 27 (1984) 1048–1050.
[69] Sreenivasan K.R., The energy dissipation in turbulent shear flows, in: Deshpande S.M., Prabhu A., Sreenivasan K.R., Viswanath P.R. (Eds), Symposium on Developments in Fluid Dynamics and Aerospace Engineering, Interline Publishers, Bangalore, 1995, pp. 159–190.
[70] Grossmann S., Lohse D., Lvolv L., Procaccia I., Finite size corrections in high Reynolds number turbulence, Phys. Rev. Lett. 73 (1994) 432–435.
[71] Wyngaard J.C., Tennekes H., Measurements of the small-scale structure of turbulence at moderate Reynolds numbers, Phys. Fluids 11 (1970) 1962–1969.
[72] Smith L.M., Reynolds W.C., The dissipation-range spectrum and the velocity derivative skewness in turbulent flows, Phys. Fluids A 3 (1991) 992–994.
[73] Manley O.P., The dissipation range spectrum, Phys. Fluids A 4 (1992) 1320–1321.
[74] Sanada T., Comment on the dissipation-range spectrum in turbulent flows, Phys. Fluids A 4 (1992) 1086–1087.
[75] Tabeling P., Zocchi G., Belin F., Maurer J., Willaime H., Probability density functions, skewness, and flatness in large Reynolds number turbulence, Phys. Rev. E 53 (1996) 1613–1621.
[76] Jimenez J., Wray A.A., Saffman P.G., Rogallo R.S., The structure of intense vorticity in isotropic turbulence, J. Fluid Mech. 255 (1993) 65–90.